Alexandria Engineering Journal (2022) 61, 763–774

HOSTED BY

ELSEVIER

Alexandria University

Alexandria Engineering Journal

www.elsevier.com/locate/aej
www.sciencedirect.com

Optimal operation of under-frequency load shedding relays by hybrid optimization of particle swarm and bacterial foraging algorithms

Hilmy Awad [a,*], Ahmed Hafez [b]

[a] *Electrical Technology Department, Faculty of Technology and Education, Helwan University University, Cairo, Egypt*
[b] *Electrical Engineering Department, Faculty of Engineering, Assiut University, Assiut, Egypt*

Received 31 January 2021; revised 30 April 2021; accepted 14 June 2021
Available online 26 June 2021

KEYWORDS

Bacterial foraging;
Hybrid optimization;
Load-shedding techniques;
Particle swarm optimization;
Swing frequency

Abstract Particle Swarm (PSO) and Bacterial Foraging (BF) Optimizers are two widely used optimization techniques. A proper combination of these two algorithms would improve their search capability while minimizing their shortcomings, such as parameter dependency and premature convergence. This paper presents a hybrid optimization algorithm that combines PSO and BF (HPSBF) to ensure security and the system's stability following faults and disturbances. The formulated objective function is claimed to be innovative and straightforward.

The set objectives are to minimize the dropped load by shedding relays while maximizing the lowermost swing frequency. The optimal operation of Under-Frequency Load-Shedding (UFLS) Relays is driven by the HPSBF technique as a bounded optimization with bounds representing the limits of the system's state variables. The viability of the HPSBF is verified against conventional-, PSO-, and BF-UFLS approaches. The standard IEEE 9-bus and IEEE 39-bus systems are exploited to examine the response of the developed UFLS techniques. The tested systems are exposed to various operational scenarios such as loss of power plants and a considerable abrupt load increase. The DigSilent power factor software is used to simulate the IEEE 9- and 39-bus systems, while MATLAB code was implemented to obtain optimal operational points for the implemented algorithms. The HPSBF accomplished the uppermost swing frequency and the lowermost quantity of the disconnected load. Furthermore, the computational times of HPSBF are equivalent to those of the PSO.

1. Introduction

For a stable operation of power systems, a balance between load and generation should be guaranteed. Among numerous techniques, load shedding is one of the effective controls that mitigate disturbances/faults in the case of a significant

* Corresponding author.
E-mail addresses: hilmy_awad@techedu.helwan.edu.eg (H. Awad), prof.hafez@aun.edu.eg (A. Hafez).

Peer review under responsibility of Faculty of Engineering, Alexandria University.

https://doi.org/10.1016/j.aej.2021.06.034
1110-0168

Nomenclature

AFC_i	Average rate of frequency change
f_{cb}	System's frequency due to the circuit-breaker reaction
f_i	System's Frequency
f_{min}	*Smallest possible swing frequency*
f_o	System's Nominal frequency
H_s	Inertial time constant
i	Stage number
L_0	Initial overload ratio
L_i	Overload load ratio at the i^{th} stage
L_{or}	Ratio of overloading
L_{rci}	Reduction coefficient of the load
L_S	Quantity of saved load from unnecessary tripping
$P_{currenti}$	Current location of bacterium i
pf	Power factor
P_{Gi}	Generated active power at stage i
P_{LD}	Initial amount of load power
P_{Li}	Active power of the Load at stage i
$P_{Litotal}P_{Litotal}$	Total active power of the load before activating of load shedding
$P_{Litotal+1}$	Updated value of the total active power
P_{LSi}	Dropped power
S	Total number of steps of load shedding
SM	Safety margin
t_d	Time delay
t_b	Circuit-breaker time
t_{di}	Decaying time
T_i, T_{imax}	Current and maximum iterative times, respectively.
v_i^k	Velocity of particle number i at the iteration k
v_i^{k+1}	Velocity of particle i^{th} the at the iteration number $k + 1$
v_{max}	Allowable maximum speed of a particle.
w_{imin}, w_{imax}	Minimum and maximum weight, respectively.
$\beta(i)$	Direction angle at stage i
δ	Percentage of load shedding

mismatch between load and generation [1–5]. The load shedding action should be activated directly after either voltage or frequency has dropped below the allowable limits. Hence, two approaches to load shedding are identified: Under-Voltage Load Shedding (UVLS) and Under-Frequency Load Shedding (UFLS). In the case of UVLS, depending on the voltage drop, the disconnected load amount at each stage is determined. The UFLS presents more accurate performance than the ULVS because the voltage deviation is not necessarily linked to the occurred disruption [5,6].

Both fixed- and adapted- step size approaches are implemented in the UFLS, classified as static and dynamic approaches. In the static approach, the fixed-step size is kept at all phases. That is straightforward, but it might result in the tripping of unnecessary customers. The dynamic approach adjusts the step size based on accurate calculations, which in turn improves the flexibility of the UFLS and increases the power supply security [5–8].

The main advantage of UFLS is that it achieves a quick recovery of the power system frequency following a severe fault or a disturbance. The traditional UFLS techniques primarily depend on comparing the operational frequency against a preset frequency level at each stage, which may activate the next stage accordingly. The amounts of the removed load and the step size could be fixed or variable. Inaccurate calculations of the removed load amount, which causes the tripping of unnecessary loads, is a significant disadvantage of such traditional techniques. Also, the erroneous determination of delay between successive stages may endanger the system's stability [5–9].

Artificial intelligence (AI) techniques have been researched for UFLS applications. They offer superior performance compared to conventional UFLS schemes in terms of adaptive step size and the highest possible lower swing frequency [10–14]. Fuzzy logic is a member of AI techniques, which requires an exact identification of the membership's parameters and functions; if not, the solution diverges from the optimum value [10,11]. Artificial Neural Networks (ANNs) present better UFLS functioning compared to Fuzzy Logic or classical UFLS. On the other hand, ANNs might not be applied in many fault/disturbance scenarios. Besides, ANNs mandate long training in the cases of complex network structures [12–14].

Optimization techniques, for instance, Genetic Algorithm [15], Ant Colony [16,17], Monte-Carlo, and others [18–25], are recently being applied to load shedding. Generally, the metaheuristic optimization can reduce the amount of removed loads and keep the lowest swing frequency maximally. But on the other hand, the convergence toward a global solution can't be guaranteed in many cases. Other disadvantages are that most of these algorithms are initial-solution dependent and vary widely in their computational requirements and execution difficulty [26–28].

The Particle Swarm Optimization (PSO) is a relatively well-experienced metaheuristic algorithm with the merits of quick convergence and robustness [21–23]. It is a stochastic-search optimization algorithm with a parallel structure that has been exploited to optimize the power system's performance and increase the stability's margin.

Another metaheuristic algorithm, the Bacterial Foraging (BF) algorithm imitates a natural phenomenon's behaviour, that is, the hunting process of *E. coli*. Bacteria. Like the PSO, BF is also a widely used optimizer [25,29].

A hybrid optimization employing PSO, and BF (HPSBF) has been proposed in the literature for various applications. For instance, the authors of [30] proposed the merging of PSO with BF to conquer the optimization delay and further enhance the performance of the BF algorithm in the case of tuning a Fractional-order PI-speed controller in a permanent magnet synchronous motor drive. In [31], a loss minimization based-HPSBF was presented to reconfigure the distribution network. Also, the HPSBF has been implemented harmonics mitigation [32] and the parameters' identification of photovoltaic modules [33].

This paper proposes a robust multi-objective Hybrid PSO and BF (HPSBF) algorithm to operate the UFLS relays optimally. The proposed optimizer merges PSO and BF's advantages, such as convergence rate and the found solution's superiority. The performance of HPSBF is extensively tested and compared to the performance of PSO, BF, and conventional UFLS methods for various disturbances., The IEEE 9-bus and IEEE 39-bus standard systems are exploited to examine the applicability and feasibility of the proposed HPSBF with disturbances such as an outage of a single plant, simultaneous outage of multiple plants, and sudden increase of the connected loads.

The proposed HPSBF optimizer is coded using Matlab, while DigSilent software is employed to investigate the response of the tested systems. The main contribution of the paper is summarized as:

- Providing a reliable and robust hybrid HPSBF for the optimal operation of UFLS relays,
- Evaluating the performance of HPSBF and comparing it to PSO, BF and traditional UFLS schemes.

Section 2 of the article presents the guidelines for tuning the UFLS relays. In Section 3, the HPSBF hybrid algorithm is explained in detail. The tested IEEE 9- and 39-bus standard systems are briefly described in Section 4. Section 5 presents the simulation results and discussions. Conclusions are given in Section 6.

2. Tuning of UFLS relays

Effective load shedding schemes require the full definition of four elements: block size of the loads to be disconnected, frequency settings, number of shedding steps, and the applied time delay between successive steps [3–5]. Here, a brief description of each element is given.

2.1. Block size of the removed load

Load shedding algorithms must differentiate the various possible disruptions in power systems. Depending on the disturbance's type and severity, the block size of the disconnected load is determined. In the case of UFLS, the value of the frequency error is the main indicative factor. Intuitively, the increase or decrease in the value of frequency error, positive or negative, reveals the disturbance's severity.

If the dropped load's block size is a fixed value over the consequent stages, unnecessary loads may be removed, reflected in economic and customer satisfaction issues. Thus, this research has given a trial to mathematically relate frequency error to the dropped load block size based on the results presented in [3–5,19].

2.2. Frequency threshold

Two thresholds are considered for each load shedding stage: 1) preset frequency; and 2) rate of frequency decay [15]. The degree of severity of the disturbance is manifested in the value of the frequency decay rate, which is primarily employed to identify the time delay of each load shedding step. The acceptable lower limit (by the grid operators) of the operational frequency specifies preset frequency value.

2.3. Number of load shedding steps

Of course, many loads cannot be removed bulkily [3] as this would worsen the system's stability. Instead, they are being dropped out of a multi-stage pattern according to accurate calculations and the load's priorities. Such estimates are mainly related to the severity and type of the disturbance. An efficient load shedding algorithm must drop the lowest amount of load and preserving the system's stability.

2.4. Time delay for each step

A time lag is applied before executing the subsequent step to record and quickly judge the system's performance after a load shedding stage. On the other hand, such a delay should be correctly identified to release the mechanical stresses on the turbine and other equipment. The time delay also depends on the type and severity of the disturbance.

A sudden loss of a large-size generator is the primary motive for applying the load shedding scheme, after such disruption, the produced power falls. The load status has not changed yet compared with its value before the disruption.

The ratio of overloading, L_{or} is given in (1) [34],

$$L_{\mathrm{or}} = \frac{\sum P_{\mathrm{Li}} - \sum P_{\mathrm{Gi}}}{\sum P_{\mathrm{Gi}}} \quad (1)$$

where L_{or} is the ratio of overloading, P_{Li} represents the amount of active power of the Load at stage i, and P_{Gi} denotes the amount of generated active power at stage i. The average rate of frequency variation, AFC_i, is written in (2) [35].

$$AFC_{\mathrm{i}} = \frac{f_{\mathrm{i}}^2\, L_{\mathrm{or}}\, pf}{H_{\mathrm{s}}} \frac{f_{\mathrm{i+1}} - f_{\mathrm{i}}}{f_{\mathrm{i}}^2 - f_{\mathrm{i+1}}} \quad (2)$$

Here H_{s} is the inertial time constant, f_{i} represents the system's frequency at the current stage, and $f_{\mathrm{i+1}}$ represents the system's frequency at the next stage. The value and sign of $\mathrm{AFC_i}$ obtained by (2) indicate the disturbance severity and type. For instance, a positive sign implies a disconnection of a generator/power plant, while a negative sign identifies a sudden rejection of a load. Furthermore, the absolute value of $\mathrm{AFC_i}$, $\mathrm{IAFC_iI}$, specifies the severity of the disruption.

The load shedding percentage, $\delta\delta$, is calculated by (3).

$$\delta = -\frac{2H_{\mathrm{s}}}{f_{\mathrm{o}}} AFC_{\mathrm{i}} \quad (3)$$

where f_{o} designates the system's nominal frequenc.

The dropped power, P_{LSi} (MW), at each step is determined by (4) in terms of the total load power (P_{Litotal}) [3].

$$P_{\mathrm{LSi}} = \delta_{\mathrm{i}}\, P_{\mathrm{Litotal}} \quad (4)$$

After the disconnection of load in a load-shedding step, an update is required about the status of the system's load. The remaining load, $P_{\mathrm{Ltotali+1}}$, is then given by,

$$P_{\mathrm{Litotal+1}} = P_{\mathrm{Litotal}} - P_{\mathrm{LSi}} \quad (5)$$

Following detection of under-frequency status, the UFLS relay instantaneously sends a tripping order to the engaged circuit breaker. This operation requires a definite amount of time, known as a delay time, $t_{di.}$ Such a time delay t_{di} has a strong influence on the system's response. Therefore, the design and operation professionals' primary objective is to reduce the time delay, t_{di}. The time delay, t_{di}, is given by [3,35],

$$t_{di} = \frac{f_{i+1} - f_i}{AFC_i} \tag{6}$$

Not only that, but the response of the contacts of the circuit-breaker introduces an added time delay because it requires non-zero time to react. This time delay usually is longer than one fundamental-frequency period and varies according to the type of installed breakers. Of course, the breaker's time response must be counted in calculations as it influences the frequency decline. The circuit-breaker time t_b is calculated according to:

$$t_b = \frac{Number\ of\ cycles\ of\ breaker's\ response}{50\ or\ 60} \tag{7}$$

Here, 50 or 60 is the power-system frequency. The system's frequency, f_{cb}, due to the breaker reaction is linked to t_b by:

$$f_{cb} = AFC_i \times t_b \tag{8}$$

The frequency error must be continuously updated to involve the breaker's response time and its frequency f_{cb} (9).

$$\Delta f_{new-i} = \Delta f_{old-i} - f_{cb} \tag{9}$$

Hence, the decay time should also be updated under such conditions, as in (10).

$$t_{d-new-i} = \frac{\Delta f_{new-i}}{AFC_i} \tag{10}$$

Let us assume a safety margin (SM) to be 200 mHz. The SM must be adjusted to provide sufficient room for decreasing the mechanical stresses on the spinning turbine and guaranteeing a proper operation. Then, the frequency of the next step is set as in (11):

$$f_{sh-i} = \Delta f_{new-i} - SM \tag{11}$$

where f_{new-i}f$_{new-i}$ is the frequency at the subsequent step of load shedding incorporating the circuit breaker's delay trip time. f_{sh-i} is the preset frequency to activate the next phase of load shedding. The reduction coefficient, L_{rci} Lrc$_i$,of the load, characterizes the proportion between load power and the system's frequency. It is calculated as given in (12).

$$L_{rci} = \frac{L_{or} - L_{or-i}}{(1 + L_{or})(1 - f_{shi}/f_o)} = \frac{1 - P_{Li}/P_{Lo}}{1 - f_{shi}/f_o} \tag{12}$$

The minor swing frequency, $f_{min,}$ f$_{min}$,denotes the minimum acceptable frequency value. It is given by (13) [35].

$$f_{min} = \left\{1 - \frac{L_{or}}{L_{rci}(L_{or} + 1)}\right\} f_0 \tag{13}$$

The principal aim of the UFLS is to boost the value of the minimum allowable frequency f_{min}f$_{min}$, which decreases the probable failures and protects the generation unit. Naturally, if the system's frequency decreases below f_{min}, the UFLS would fail to reestablish the system's stability [35].

3. HPSBF for UFLS

The main objectives of the proposed hybrid HPSBF are to:

1. minimize the amount of the removed load while preserving the stability of the system.
2. maximize the lowermost possible swing frequency.

Thus, the proposed hybrid optimization algorithm is claimed as a multi-objective algorithm expecting to merge few merits such as diversity of the search, quick convergence, and high-quality solution. It would also avoid local trapping. In this section, a brief review of BF and PSO is given.

3.1. PSO technique

A population of particles is distributed in a multi-dimensional search space. The positions and velocities of the particles are arbitrarily chosen [22–24]. The particle's velocity is given in (14).

$$v_i^{k+1} = w_i \times v_i^k + c_1 \times rand\left(pbest_i - S_i^k\right) + c_2 \times rand\left(gbest - S_i^k\right) \tag{14}$$

where:

$pbest_i$ is the best location for the i^{th} particle at the k^{th} iteration.
$gbest$ is the best position globally of the group so far.
S_i^k is the present position of i^{th} particle.
c_1 and c_2 are typically chosen in the range from 0.5 to 2.0 [24].
w_i the assigned inertial weight of the i^{th} particle, typically assigned in the range from 0.4 to 0.9 [23,24]. w_i is calculated as in (15).

$$w_i = w_{i\,max} - \frac{w_{i\,max} - w_{i\,min}}{T_{i\,max}} T_i \tag{15}$$

The maximum velocity of i^{th} particle is expressed as:

$$v_i^{k+1} = \begin{cases} v_i^{k+1} & \left|v_i^{k+1}\right| < v_{max} \\ v_{max} & v_i^{k+1} \geqslant v_{max} \\ -v_{max} & v_i^{k+1} \leqslant -v_{max} \end{cases} \tag{16}$$

S_i^{k+1} is the updated position of a particle given in (17).

$$S_i^{k+1} = S_i^k + v_i^{k+1} \tag{17}$$

The objective function is calculated for i^{th} particle and then compared to $pbest_i$. Subsequently, $pbest_i$ is compared to $gbest$ to improve all the particles' movement experience. If a particle member has a better position compared to $gbest$, this position is then stored. Consequently, $gbest$ is then updated. This procedure would continue until convergence to the global best position is realized or the predefined iteration numbers are reached.

3.2. BF technique

The BF algorithm depends on the implementation of the group-hunting approach of the *E-coli* bacteria swarms. BF requires four main steps: chemotaxis, swarming, reproduction, and elimination dispersal [25,29].

i. Chemotaxis

Chemotaxis is usually the procedure at which a bacterium swims and scans in tiny steps whilst looking for nutrients. In a BF algorithm, chemotaxis identifies the location of the i^{th} bacterium, $\theta^i(j+1, k, l)$, corresponding to the step size $c(i)$ and the current position $\theta^i(j, k, l)$ at j^{th} chemotactic, k^{th} reproductive and l^{th} elimination-diffusion step.

$$\theta^i(j+1,k,l) = c(i) \times \beta(i) + \theta^i(j+1,k,l) \tag{18}$$

$$\beta(i) = \triangle(i)/\sqrt{\triangle^{T}(i)\triangle(i)} \tag{19}$$

Δ represents an arbitrary direction vector whose components lie in the range from −1 to 1 [25].

ii. Swarming

It denotes the group's conduct of numerous motile varieties as the E-coli bacteria in reordering. The reordering is done in complicated and stable Spatio-temporal forms (swarms) in a semisolid nutrient environment. When a set of *E-coli* cells is in a semisolid matrix along with a single nutrient chemo-effector, they organize themselves in a circle via pushing up the nutrient gradient. If they are motivated by a high level of succinate, such cells circulate an attractant aspartate that aids them to be collected into groups. Thus, they move in concentric forms of swarms with a high-level bacterial concentration. The cell-to-cell signalling in *E-coli* swarm is given by (20) [29,35].

$$\begin{aligned} j_{cc}(\theta, p(j,k,l)) &= \sum_{i=1}^{s} j_{cc}\left(\theta,\ \theta^i(j,k,l)\right) \\ &= \sum_{i=1}^{s} -d_{\text{attracant}}\, e^{-\omega_{\text{attracant}} \sum_{i=1}^{p}\left(\theta_m-\theta_m^i\right)^2} \left(\theta,\ \theta^i(j,k,l)\right) \\ &+ \sum_{i=1}^{s} h_{\text{repellant}}\, e^{-\omega_{\text{repellant}} \sum_{i=1}^{p}\left(\theta_m-\theta_m^i\right)^2} \left(\theta,\ \theta^i(j,k,l)\right) \end{aligned} \tag{20}$$

In order to formulate a time-dependent objective function, $j_{cc}(\theta,p(j,k,l))$ is added to the main objective function. The terms in (20) are defined below.

S is the overall quantity of bacteria.
p denotes the number of optimized variables in each bacterium.
$\theta = [\theta,\ \theta_1,\ldots\ldots,\theta_p]^T$ represents a point in the search domain (p-dimensional)[29].
$h_{attracant}$ is the strength of attractant that delivered by the cell.
$\omega_{attracant}$ is an indication of the width of the attractant.
$h_{repellant}$ designates the height of the repellant's impact.

$\omega_{repellant}$ represents an indication of the width of the repellant.

iii. Reproduction

Reproduction in BF describes the natural choice in other optimization methods, where the lowest healthy bacteria ultimately die. In contrast, every most healthy bacteria is replicated into two bacteria in an asexual reproduction approach. They are allotted in exact locations to maintain swarm size. Here, the objective function gives a measure of the swarm's health. Members that have a small objective-function value are considered the healthy ones.

iv. Elimination and Dispersal

Obviously, when the bacteria get unexpected variations in their community, such as a substantial increase in the temperature, the elimination or dispersal would happen. This procedure is inspired in BF by randomly liquidating a few bacteria with a little likelihood P_{ed}, while a new substitute is arbitrarily adjusted in the search space. The main aim of the dispersal is to stop tripping at a regional minimum; though, it could disrupt the optimization procedure. Frequently, the scattering happens after a specific number of reproduction developments [25,29].

3.3. Modeling of HPSBF technique

In the HPSBF algorithm, the velocity calculation of PSO is utilized to estimate the updated chemotaxis drop direction in the BF algorithm. Thus, the unity-length random order of a tumble's performance can be adapted to the best global position besides the individual's best position (21).

$$\begin{aligned} \beta(j+1) &= w_i \times \beta(j) + rand(pbest_i - p_{current\ i}) \times c_1 \\ &+ rand(gbest - p_{current\ i}) \times c_2 \end{aligned} \tag{21}$$

3.4. Objective function

As stated earlier, the suggested objective function must satisfy dual objectives: 1) minimize the quantity of removed load and 2) maximize the lowest possible swing frequency. Here, the objective function is formulated as in (22).

$$f_{HPSBF} = \min\left\{w_1|u_\delta(\delta,\ s,\ t_d,\ P_L)| + w_2\left|v_{f\min}(\delta,\ s,\ t_d,\ P_L)^{-1}\right|\right\} \tag{22}$$

where

u_δ and $v_{f\min}$ are functions of the block size and the lowest possible swing frequency, respectively.
w_1 and w_2 are two weight coefficients that are identified as,

$$w_1 + w_2 = 1,\ w_1 \in [0,1], \quad \text{and} \quad w_2 \in [0,1] \tag{23}$$

w_1 and w_2 are selected to ensure that the objectives are located far enough from the region of large variations. The quantity of the disconnected load has a more substantial influence than the minimum allowable swing frequency. Consequently, in this research, $w_1 = 0.68$ and $w_2 = 0.32$.

The function f_{HPSBF}, (22) is claimed to be innovative and straightforward. Eq. (22) is subjected to several constraints that comprise a percentage of permissible load shedding, power flow boundaries, number of load-shedding steps, and time delay applied between the steps. These constraints are stated in Eqs. (24) to (27).

$$P_{\mathrm{Lmin}\,i} < P_{\mathrm{L}\,i} \leqslant P_{\mathrm{Lmax}\,i} \tag{24}$$

$$\delta_{\min} < \delta \leqslant \delta_{\max} \tag{25}$$

$$S_{\min} < S \leqslant S_{\max} \tag{26}$$

$$t_{\mathrm{dmin}} < t_{\mathrm{d}} \leqslant t_{\mathrm{dmax}} \tag{27}$$

where

$P_{\mathrm{L}i}$, $P_{\mathrm{Lmax}\ i}$ and $P_{\mathrm{Lmin}\ i}$ $\mathrm{P}_{\mathrm{L\,min\,i}}$ represent the active load power at bus number i and its limits.
δ, $\delta_{\max}$, and $\delta_{\min}$ denote the percentage of permissible load shedding and its limits.
S, $S_{\max}$, and $S_{\min}$ are the number of tolerable shedding steps and their limits.
t_{d}, t_{dmax}, and t_{dmin} designate the that should be applied between successive stages and its limits.

4. Tested systems

The standard IEEE 9- and the IEEE 39-bus systems are exploited to prove the HPSBF's applicability and effectiveness at various UFLS applied techniques. Fig. 1 displays the IEEE 9-bus [36], where bus 1 is set as the slack bus. G_1, G_2 and G_3 have the capacities of 247.5, 163.2, and 108.8 MW, respectively. The loads at buses 5, 6, and 8 will be detached whose capacities are 125, 90, and 100 MW.

The IEEE 39-bus is shown in Fig. 2 [37]. It consists of 10 power plants, 46 transmission lines, and 29 load buses. The aggregate capacity of the IEEE 39-bus system is 6140.80 MW. The capacities of the generators ordered from 1 to 10 are 1000.0, 520.81, 650.0, 632.0, 508.0, 650.0, 560.0, 540.0, 830.0 and 250.0 MW, respectively. The total connected load is about 6097.1 MW. Bus number 39 is taken as the slack bus.

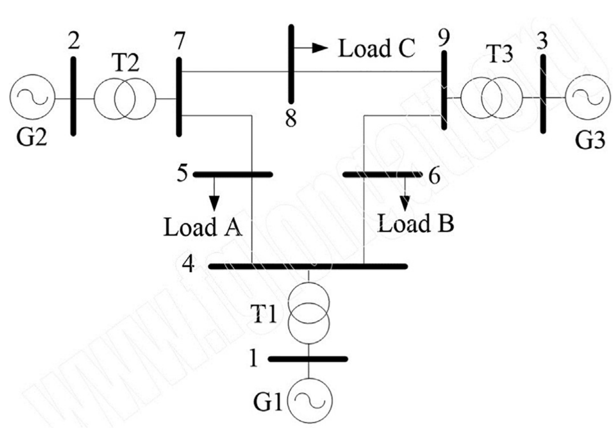

Fig. 1 Single-line diagram of IEEE 9-bus system.

5. Simulation Results and discussions

Six cases are applied to confirm the effectiveness of the suggested UFLS optimization technique. These cases introduce severe disturbances, such as several outages of generation stations and abrupt load increase. The investigated cases include:

I. Sudden drop of G_1 is suddenly dropped in the 9-bus system
II. Simultaneous outage of G_2 and G_3 in the 9-bus system
III. Abrupt load increase in the 9-bus system
IV. Simultaneous outage of G_1, G_3, and G_9 in the 39-bus system.
V. Simultaneous outage of G_1, G_7 and G9 in the 39-bus system.
VI. Sudden load surge in the 39-bus system.

For each case, conventional, PSO, BF, and HPSBF are exploited to set the UFLS relay. In each case, the following parameters are computed for all UFLS applied algorithms:

- percentage of load shedding, δ
- lowest possible operational frequency $f_{\min}$
- percentage of unnecessary load shedding prevention
- total number of load shedding steps, s
- time delay, t_{d}

5.1. Traditional UFLS method

In the conventional UFLS approach, the threshold system's frequency for each step and its deviation Δf are the required inputs considering that the minimum possible of the operational frequency is the first stage's threshold. For 50-Hz systems, the value of 49.2 Hz is typically adopted as a threshold for the first stage [5–8], and thus, it is used in the presented work. To determine the settings of the UFLS relays, the dynamic equations of the system are used in the DigSilent software package.

Here, when one step of UFLS was applied, the system was incapable of maintaining its stability. So, a multi-stage shedding was implemented. The investigated systems (with the proposed UFLS techniques) are simulated using the DigSilent software with the Mid-term RMS simulation. Optimal operating points have been obtained via coding of the various UFLS procedures Matlab Package Software.

5.2. Case 1: Sudden drop of G1 is suddenly dropped in the 9-bus system

The outage of G_1 is considered here at time = 4 s while activating the load shedding at t = 4.87 s. The simulation results are presented in Table 1. The outage of G_1 is a severe disruption, which dictates the activation of load shedding to retain system security, reliability, and continuity of at least for sensitive loads. All applied UFLS methods have successfully implemented the load shedding and preserved the system's stability. Fig. 3 shows the time response of the systems' frequency following the applied disruption

HPSBF offers improved performance compared to PSO and BF. It provides about 0.41 and 0.33% increase in the

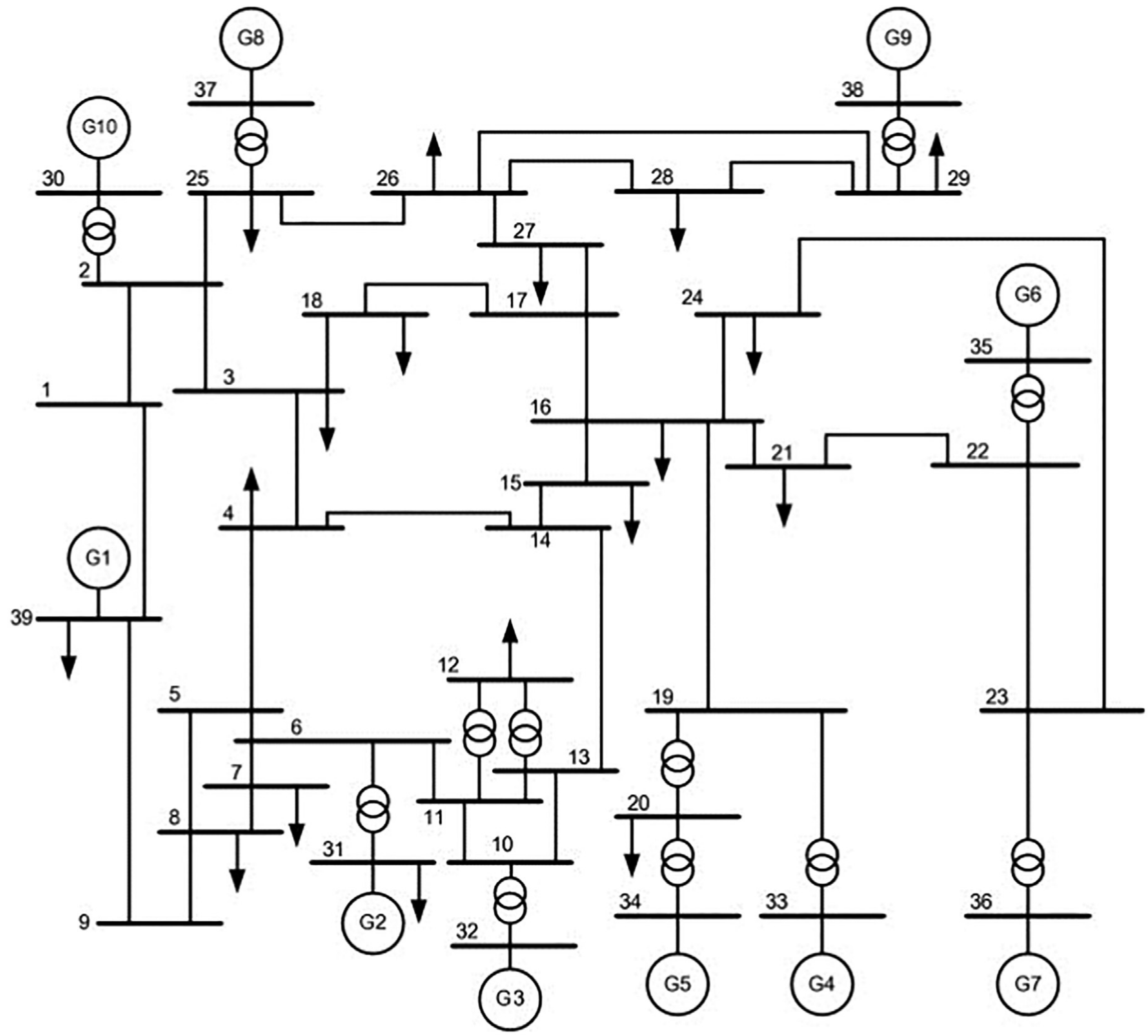

Fig. 2 Single-line diagram of the standard IEEE 39-bus system.

Table 1 Results of Case 1: outage of G_1 in the IEEE 9-BUS system.

Algorithm	Parameters				
	δ (%)	f_{min} (Hz)	L_S (%)	S	t_d (ms)
Traditional	47.8	48.21	–	4	353
PSO	42.5	48.42	5.31	8	171
BF	41.2	48.40	6.59	8	171
HPSBF	37.1	48.58	10.70	10	132

swing frequency than PSO and BF, respectively. Also, HPSBF guarantees that 31.5 MW of the loads are saved.

5.3. Case II: Simultaneous outage of G_2 and G_3 in the 9-bus system

In this case, G_2 and G_3 are detached at the time of 4 s, and the load-shedding is activated at 4.612 s. The findings are illustrated in Table 2.

Dropping of both G_2 and G_3 is a highly substantial disturbance for the IEEE 9-bus system, as these two stations produce about 52% of total power. Generally, the IEEE 9-bus is of restricted manoeuvrability, as only three generators produce its power. A complete loss of G_1 simultaneously with any other generator would result in a black-out.

The results presented in Table 2 reveal that all the applied UFLS techniques can successfully reestablish the system's stability following such a significant disruption. However, PSO, BF, and HPSBF techniques can lower the amount of removed load because they apply more load-shedding steps than the conventional method, reducing the dropped load. It is evident from Table 1 that HPSBF has a better performance compared to the PSO and BF algorithms in terms of the amount of dropped load and the swing frequency.

Fig. 4 displays the time response of the system's frequency of the 9-bus system in the applied disturbance with traditional, PSO, BF, and HPSBF techniques. The frequency suffers a significant fall, as the lowermost swing frequency reaches about 48.01 Hz, which is very close to the border of the primary frequency control. Fig. 4 also displays that traditional and meta-heuristic algorithms can successfully reinstate the system's

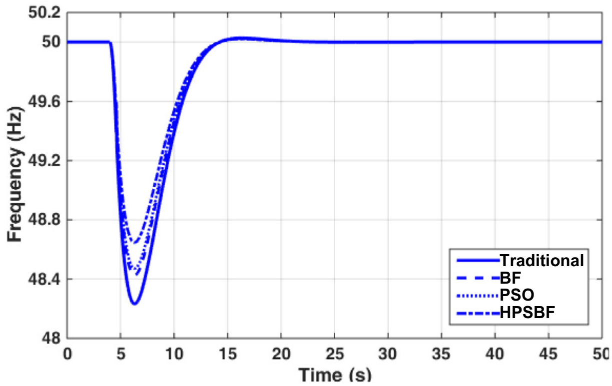

Fig. 3 Time response of the 9-bus system's frequency in case of outage of G_1.

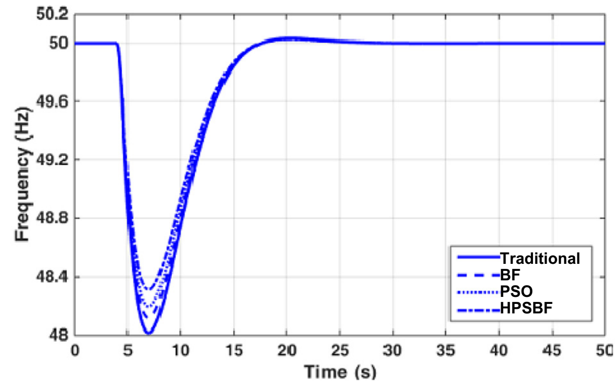

Fig. 4 Time response of the 9-bus system's frequency in case of outage of G1 and G2.

stability with the minimum number of shedding stages. However, the dynamic responses of the various applied techniques are comparable.

A quick comparison between Figs. 3 and 4 shows that Case 2 is more severe than Case 1, as the lowermost swing frequency in Case 1 is considerably higher than that in Fig. 4.

5.4. Case 3: Abrupt load surge in the 9-bus system

Here, a 100% surge in the connected load at bus 5 is abruptly applied. As the total load is 440 MW, the sudden rise is about 42%, which should activate the load shedding procedure. The load surge is applied at 4 s, and then the load shedding is triggered at 4.92 s. The simulation results of traditional, PSO, BF, and HPSBF are given in Table 3.

Conventional UFLS algorithm causes tripping of about 7.34 MW. However, metaheuristic techniques keep the initial load without any load removal. Besides, they permit the system operation under slight overloaded as given in Table 3. Table 3 indicates that the UFLS algorithms can effectively sustain system stability and validate UFLS approaches' functionality in this case of load increase. HPSBF delivers the uppermost lowest possible swing frequency and the minor detached loads, as evident in Table 3.

The time response of the system's frequency of the investigated case (100% surge in the load at bus number 5) is depicted in Fig. 5 with the various UFLS techniques. The nominal frequency after the sudden load increase has been restored. HPSBF still dominates the other applied optimization techniques. The HPSBF produces the highest lowermost swing frequency (shown in Fig. 5) while limiting the dropped load.

5.5. Case 4, Simultaneous outage of G_1, G_3, and G_9 in the IEEE 39-bus system

Different cases can be examined in the IEEE 39-bus system. Nevertheless, in this research, a top priority is offered to the concurrent outage of G_1, G_3, and G_9. G_1 and G_9 are the largest power plants, and thus they are involved in this case. The circuit breakers of these generators are opened at 6 s, and the load shedding is commenced at 6.91 s. The simulation outcomes are illustrated in Table 4.

The HPSBF keeps more loads in operation compared to PSO and BF, as illustrated in Table 4. Additionally, it yields a higher lowermost swing frequency, but the number of shedding stages has increased. The increased number of stages in HPSBF is attributed to the target of preserving system stability and at the same time raising the lower boundary of the frequency level throughout trouble.

The time response of the system's frequency of the IEEE 39-bus system in the case of simultaneous outages of G_1, G_3 and G_9 with the implemented UFLS techniques are depicted in Fig. 6, in which the effectiveness of the applied UFLS techniques in restoring system stability (under such severe trouble) is proved. The long-lasting time of the disturbance is attributed to the disturbance severity and the response of the loads.

5.6. Case 5: Simultaneous of G1, G7, and G9 in the IEEE 39-bus system

In Case 5, G_1, G_7 and G_9 are disconnected at 6 s, and the shedding is begun at 6.95 s. G_1, G_7, and G_9 produce around 38% of

Table 2 Results of case 2: Simultaneous outage of G_2 and G_3 in the 9-bus system.

Algorithm	Parameters				
	δ (%)	f_{min} (Hz)	L_S (%)	S	t_d (ms)
Traditional	51.8	48.01	–	4	597
PSO	45.1	48.18	6.72	8	285
BF	44.6	48.11	7.22	8	285
HPSBF	43.4	48.28	8.43	11	185

Table 3 Results of case III: Load Rise At Bus 5 in the 9-BUS system.

Algorithm	Parameters				
	δ (%)	f_{min} (Hz)	L_S (%)	S	t_d (ms)
Traditional	32.35	48.32	–	4	272
PSO	26.04	48.44	6.31	8	134
BF	27.30	48.42	5.05	9	121
HPSBF	25.28	48.68	7.07	11	85

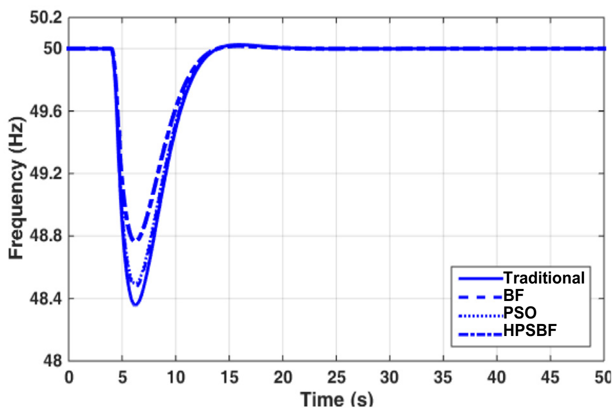

Fig. 5 Time response of the 9-bus system's frequency for abrupt load increase.

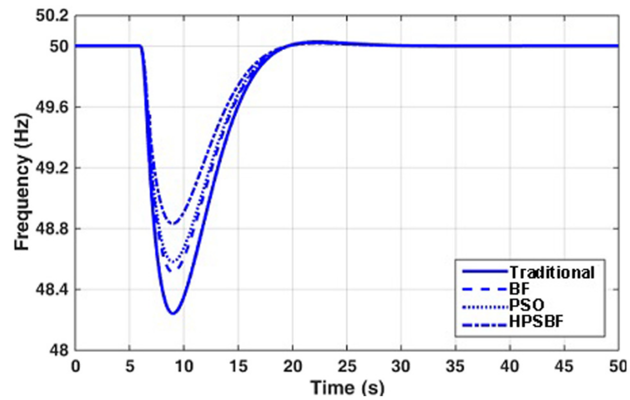

Fig. 6 Time response of the 39-bus system's frequency in case of G_1, G_3, and G_9 outage.

their outage's total capacity is a severe disturbance. The simulation outcomes are provided in Table 5.

Results displayed in Table 5 continue showing the merits of HPSBF in improving the value of the lowermost swing frequency and survival of extra loads.

Likewise, HPSBF applies the shortest time delay between successive steps, which assists in relieving the rotational masses by minimizing the mechanical stresses. The HPSBF takes a more significant number of steps compared to the other applied UFLS approaches. This is done to reduce the amount of disconnected load and to increase the lower boundary of the system's frequency.

In Fig. 7, the time response of the system's frequency is displayed for the 39-bus system in the concurrent outage of G_1, G_9, and G_7. All the different UFLS techniques (even the traditional one) restore the system's stability during and after the outage event. Again, the HPSBF has the best overall performance. Comparing Fig. 6 to Fig. 7 yields that Case 4 applies a more substantial impact on the IEEE 39-bus system than Case 5, as recognized by the level of power deficiency in Case 4.

5.7. Case 6: Sudden load surge in the 39-bus system

In Case 6, the active power at all buses is increased abruptly by 25%. Hence, the system's load becomes 7625 MW. The load surge is applied at the time of 6 s, and load shedding is triggered at 6.92 s. The simulation results are shown in Table 6. No surprise, the HPSBF still dominates other used UFLS techniques.

The time response of the system's frequency of the IEEE 39-bus system after a 25% abrupt load increase at all buses for all UFLS approaches is depicted in Fig. 8. The response is quite similar to the previous cases considering the number of disconnected loads and the swing frequency.

5.8. HPSBF versus PSO and BF

Figs. 3 to 8 confirm the viability and functionality of the applied HPSBF. The HPSBF has realized a superior performance in terms of the lowermost quantity of the disconnected load and the uppermost lowest possible swing frequency. The HPSBF technique has converged more effectively to the global solution.

The changes of the function f_{HPSBF} versus the iteration number for the cases of the 9-bus system are displayed in Fig. 9, and for the 39-bus system are shown in Fig. 10.

Figs. 9 and 10 illustrate that the PSO algorithm has provided comparatively quicker convergence than both the BF and the HPSBF algorithms. Though, BF and HPSBF own better mechanisms for preventing local optimal tripping than the PSO.

The computational times in the cases are presented in Table 7. The PSO provides the shortest computational time. HPSBF has a relatively shorter computational compared to the BF. Achieving a shorter computational time is attributed to the combined effect between BF and PSO. Of course, those computational times reported here may differ according to the abilities of the exploited processing machines.

Table 4 Results of case 4: Simultaneous of G1, G3, and G9 in the IEEE 39-bus system.

Algorithm	Parameters				
	δ (%)	f_{min} (Hz)	L_S(%)	S	t_d (ms)
Conventional	42.1	48.21	–	4	425
PSO	38.0	48.52	4.21	9	178
BF	37.5	48.46	4.70	9	189
HPSBF	33.8	48.84	8.48	10	152

Table 5 Results of case 5: Outage of G_1, G_7 and G_9 in the IEEE 39-BUS system.

Algorithm	Parameters				
	δ (%)	f_{min} (Hz)	L_S (%)	S	t_d (ms)
Conventional	36.3	48.42	–	4	225
PSO	31.8	48.71	4.50	8	101
BF	31.2	48.63	5.01	8	112
HPSBF	28.9	48.82	7.40	11	82

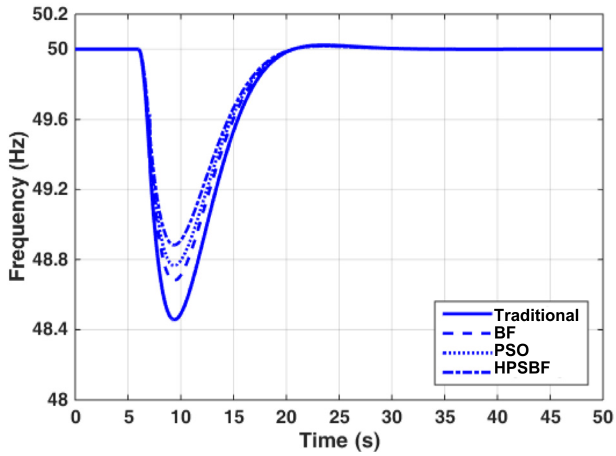

Fig. 7 Time response of the 39-bus system's frequency in case of outage of G_1, G9, and G_7.

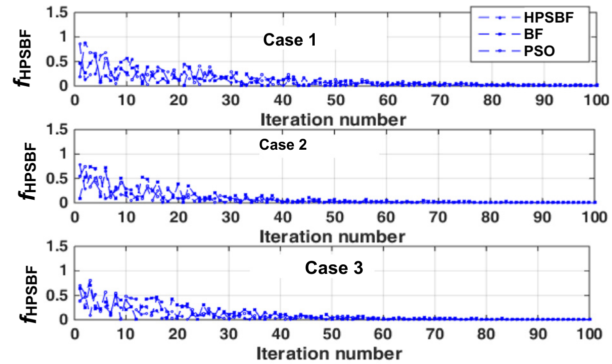

Fig. 9 Calculated values of the function f_{HPSBF} vs. iteration number for BF(circle), PSO (star) , and HPSBF (diamond) for the IEEE 9-bus system.

Table 6 Results of case 6: 25% LOAD Surge by at all buses in the IEEE 39-BUS system.

Algorithm	Parameters				
	δ (%)	$f_{\min}$ (Hz)	L_S (%)	S	t_d (ms)
Traditional	30.5	48.25	–	3	267
PSO	21.5	48.52	8.46	8	952
BF	20.8	48.56	9.64	8	1015
HPSBF	18.6	48.84	11.8	10	801

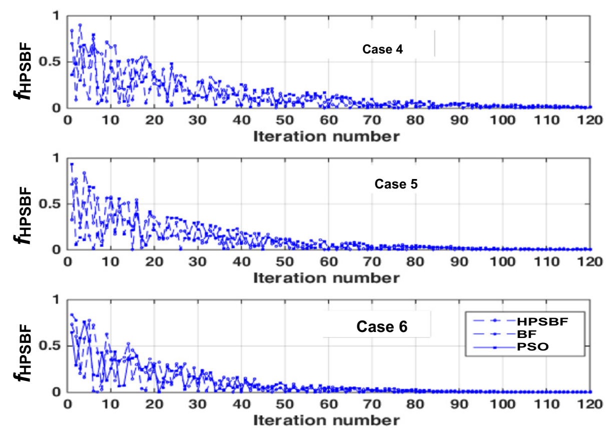

Fig. 10 Calculated values of the function f_{HPSBF} vs. iteration number for BF (circle), PSO (star), and HPSBF (diamond) for the IEEE 39-bus system.

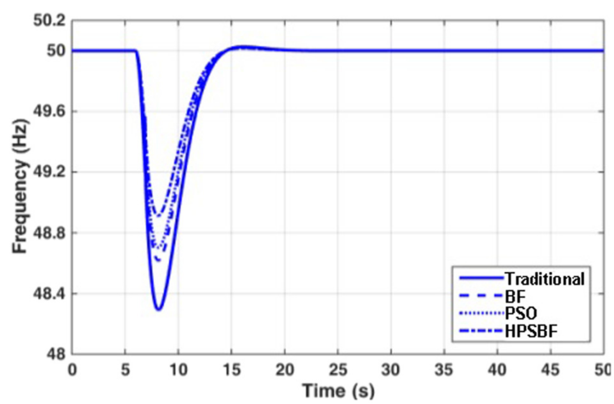

Fig. 8 Time response of the 39-bus system's frequency in case of 25% for load increase.

Table 7 Computational Times of applied algorithms.

Algorithm	Computational times of applied Cases (ms)					
	1	2	3	4	5	6
Traditional	90	84	80	124	110	107
PSO	48	45	40	75	69	65
BF	62	59	55	88	80	78
HPSBF	53	51	47	82	74	73

6. Conclusions

Various UFLS optimization techniques have implemented in this paper, including *meta*-heuristic approaches. A Multi-objective optimization that is based on a combination of PSO and BF has been developed. The objectives of the optimization algorithms are reducing the amount of disconnected load and boosting the lowest possible swing frequency. The performance merits of HPSBF are confirmed compared to the BF and PSO for several cases of disturbance in standard IEEE 9- and 39-bus systems. The HPSBF technique offered the smallest amount of the disconnected load among the other applied and achieved the uppermost lowest possible swing frequency. Considering the economic impact of the proposed algorithm, it has saved 11.9% (maximum saving) of the removed load in case 6 and 7.4% in case 5 (minimum saving). Assuming a total load of Egypt as 25000 MW, the proposed algorithm can save 2975 MW which is a substantial saving.

Declaration of Competing Interest

The authors declare that they have no known competing financial interests or personal relationships that could have appeared to influence the work reported in this paper.

References

[1] Q. Li, Y. Xu, C. Ren, A hierarchical data-driven method for event-based load shedding against fault-induced delayed voltage recovery in power systems, IEEE Trans. Ind. Informatics. 17 (2021) 699–709, https://doi.org/10.1109/TII.2020.2993807.

[2] M.E. Jabian, R. Funaki, J. Murata, Consumer appliance-level load shedding optimisation for real-time application, J. Eng. 2020 (2020) 1103–1111, https://doi.org/10.1049/joe.2019.0955.

[3] S.R.B. Y. G. Paithankar, Fundamentals of Power System Protection - Y. G. Paithankar, S. R. Bhide - Google Books, PHI Learn. Pvt. Ltd. (2011). https://books.google.com.eg/books?id=1E-lzwq5J-MC&printsec=frontcover&source=gbs_ge_summary_r&cad=0#v=onepage&q&f=false (accessed April 24, 2021).

[4] M. Klaric, I. Kuzle, S. Tesnjak, Example of undervoltage load shedding implementation, in: IEEE AFRICON Conf., 2007, https://doi.org/10.1109/AFRCON.2007.4401446.

[5] L. Sigrist, I. Egido, L. Rouco, A method for the design of UFLS schemes of small isolated power systems, IEEE Trans. Power Syst. 27 (2012) 951–958, https://doi.org/10.1109/TPWRS.2011.2174448.

[6] W. Tan, C. Shen, X. Zhang, J. Ni, A new under-frequency load shedding scheme based on OBDD, in: 1st Int. Conf. Sustain. Power Gener. Supply, SUPERGEN '09, 2009. https://doi.org/10.1109/SUPERGEN.2009.5348375.

[7] H. Jiang, G. Yan, H. Ji, L. Liu, D. Shan, An improved under frequency load shedding scheme based on rate of change of frequency, in: Proc. - Int. Conf. Electr. Control Eng. ICECE 2010, 2010, pp. 3292–3295, https://doi.org/10.1109/iCECE.2010.803.

[8] H. Mohamad, S. Sahdan, N.N.Y. Dahlan, N.M. Sapari, Under-frequency load shedding technique considering response based for islanding distribution network connected with mini hydro, in: Proc. 2014 IEEE 8th Int. Power Eng. Optim. Conf. PEOCO 2014, IEEE Computer Society, 2014, pp. 488–493. https://doi.org/10.1109/PEOCO.2014.6814478.

[9] A. Derviskadic, Y. Zuo, G. Frigo, M. Paolone, Under Frequency Load Shedding based on PMU Estimates of Frequency and ROCOF, in: Proc. - 2018 IEEE PES Innov. Smart Grid Technol. Conf. Eur. ISGT-Europe 2018, Institute of Electrical and Electronics Engineers Inc., 2018. https://doi.org/10.1109/ISGTEurope.2018.8571481.

[10] O. Shariati, A.A. Mohd Zin, A. Khairuddin, M. Pesaran, M.R. Aghamohammadi, An integrated method for under frequency load shedding based on hybrid intelligent system-part II: UFLS design, in: Asia-Pacific Power Energy Eng. Conf. APPEEC, 2012. https://doi.org/10.1109/APPEEC.2012.6307692.

[11] E. Çam, Application of fuzzy logic for load frequency control of hydroelectrical power plants, Energy Convers. Manag. 48 (2007) 1281–1288, https://doi.org/10.1016/j.enconman.2006.09.026.

[12] J. Yan, C. Li, Y. Liu, Adaptive load shedding method based on power imbalance estimated by ANN, in: IEEE Reg. 10 Annu. Int. Conf. Proceedings/TENCON, Institute of Electrical and Electronics Engineers Inc., 2017, pp. 2996–2999. https://doi.org/10.1109/TENCON.2017.8228375.

[13] C.T. Hsu, H.J. Chuang, C.S. Chen, Artificial neural network based adaptive load shedding for an industrial cogeneration facility, in: Conf. Rec. - IAS Annu. Meet. (IEEE Ind. Appl. Soc., 2008. https://doi.org/10.1109/08IAS.2008.137.

[14] F. Hashiesh, H.E. Mostafa, M.M. Mansour, A.R. Khatib, I. Helal, Wide area transient stability prediction using on-line artificial neural networks, in: 2008 IEEE Electr. Power Energy Conf. - Energy Innov., 2008. https://doi.org/10.1109/EPC.2008.4763308.

[15] W.M. Al-Hasawi, K.M. El Naggar, Optimum steady-state load-shedding scheme using genetic based algorithm, in: Proc. Mediterr. Electrotech. Conf. - MELECON, 2002, pp. 605–609. https://doi.org/10.1109/melecon.2002.1014664.

[16] N.E.Y. Kouba, M. Menaa, M. Hasni, M. Boudour, Optimal load frequency control based on artificial bee colony optimization applied to single, two and multi-area interconnected power systems, in: 3rd Int. Conf. Control. Eng. Inf. Technol. CEIT 2015, Institute of Electrical and Electronics Engineers Inc., 2015. https://doi.org/10.1109/CEIT.2015.7233027.

[17] V. Shanmugasundaram, Artificial bee colony algorithm based automatic generation control in two-area non-reheat thermal power system using SMES, in: IEEE Int. Conf. Power, Control. Signals Instrum. Eng. ICPCSI 2017, Institute of Electrical and Electronics Engineers Inc., 2018, pp. 2126–2130. https://doi.org/10.1109/ICPCSI.2017.8392092.

[18] E.J. Thalassinakis, E.N. Dialynas, A Monte-Carlo simulation method for setting the underfrequency load shedding relays and selecting the spinning reserve policy in autonomous power systems, IEEE Trans. Power Syst. 19 (2004) 2044–2052, https://doi.org/10.1109/TPWRS.2004.835674.

[19] U. Rudez, R. Mihalic, WAMS-Based Underfrequency Load Shedding with Short-Term Frequency Prediction, IEEE Trans. Power Deliv. 31 (2016) 1912–1920, https://doi.org/10.1109/TPWRD.2015.2503734.

[20] L. Shun, L. Qingfen, W. Jiali, Dynamic optimization of adaptive under-frequency load shedding based on WAMS, in: Proc. 2016 IEEE Inf. Technol. Networking, Electron. Autom. Control Conf. ITNEC 2016, Institute of Electrical and Electronics Engineers Inc., 2016: pp. 920–926. https://doi.org/10.1109/ITNEC.2016.7560496.

[21] H. Mohamad, A.I.M. Isa, Z.M. Yasin, N.A. Salim, N.N.A.M. Rahim, Optimal load shedding technique for an islanding distribution system by using Particle Swarm Optimization, in: 3rd Int. Conf. Power Gener. Syst. Renew. Energy Technol. PGSRET 2017, Institute of Electrical and Electronics Engineers Inc., 2017, pp. 154–158. https://doi.org/10.1109/PGSRET.2017.8251819.

[22] N.Z. Saharuddin, I.Z. Abidin, H. Bin Mokhlis, Intentional Islanding Solution Based on Modified Discrete Particle Swarm Optimization Technique, in: 2018 IEEE 7th Int. Conf. Power Energy, PECon 2018, Institute of Electrical and Electronics Engineers Inc., 2018, pp. 399–404. https://doi.org/10.1109/PECON.2018.8684097.

[23] S. Roy, S. Goswami, A. Pal, A. Kumar, H.K. Singh, M. Biswas, B.K. Ghosh, R.K. Mandal, Application of Modified Particle Swarm Optimization Technique for Economic Scheduling of a Complex Micro Grid with Renewable Energy Sources, in: Proc. 2nd Int. Conf. Trends Electron. Informatics, ICOEI 2018, Institute of Electrical and Electronics Engineers Inc., 2018, pp. 77–83. https://doi.org/10.1109/ICOEI.2018.8553902.

[24] J. Chen, F. Ye, T. Jiang, Numerical analyses of three inertia-weight-improvement-based particle swarm optimization algorithms, in: 2017 2nd IEEE Int. Conf. Comput. Intell. Appl. ICCIA 2017, Institute of Electrical and Electronics Engineers Inc., 2017, pp. 150–154. https://doi.org/10.1109/CIAPP.2017.8167198.

[25] W.N.E.A. Wan Afandie, T.K.A. Rahman, Z. Zakaria, Optimal load shedding using Bacterial Foraging Optimization Algorithm, in: Proc. - 2013 IEEE 4th Control Syst. Grad. Res. Colloquium, ICSGRC 2013, IEEE Computer Society, 2013, pp. 93–97. https://doi.org/10.1109/ICSGRC.2013.6653282.

[26] A. Al Mamun, M. Sohel, N. Mohammad, M.S. Haque Sunny, D.R. Dipta, E. Hossain, A Comprehensive review of the load forecasting techniques using single and hybrid predictive models, IEEE Access. 8 (2020) 134911–134939, https://doi.org/10.1109/ACCESS.2020.3010702.

[27] D. Rwegasira, I. Ben Dhaou, A. Kondoro, A. Kelati, N. Mvungi, H. Tenhunen, Load-shedding techniques for microgrids: A comprehensive review, Int. J. Smart Grid Clean Energy. 8 (2019) 341–353, https://doi.org/10.12720/sgce.8.3.341-353.

[28] C.N. Raghu, A. Manjunatha, Assessing effectiveness of research for load shedding in power system, Int. J. Electr. Comput. Eng. 7 (2017) 3235–3245, https://doi.org/10.11591/ijece.v7i6.pp3235-3245.

[29] Y. Shao, H. Chen, Cooperative bacterial foraging optimization, in: FBIE 2009 - 2009 Int. Conf. Futur. Biomed. Inf. Eng., 2009, pp. 486–488. https://doi.org/10.1109/FBIE.2009.5405806.

[30] A. Rajasekhar, R.K. Jatoth, A. Abraham, V. Snasel, A novel hybrid ABF-PSO algorithm based tuning of optimal FOPI speed controller for PMSM drive, in: Proc. 2011 12th Int. Carpathian Control Conf. ICCC'2011, 2011, pp. 320–325. https://doi.org/10.1109/CarpathianCC.2011.5945872.

[31] T. Zang, Z. He, D. Ye, Bacterial foraging optimization algorithm with particle swarm optimization strategy for distribution network reconfiguration, in: Lect. Notes Comput. Sci. (Including Subser. Lect. Notes Artif. Intell. Lect. Notes Bioinformatics), Springer, Berlin, Heidelberg, 2010, pp. 365–372. https://doi.org/10.1007/978-3-642-13495-1_45.

[32] S.S. Patnaik, A.K. Panda, Particle swarm optimization and bacterial foraging optimization techniques for optimal current harmonic mitigation by employing active power filter, Appl. Comput. Intell. Soft Comput. 2012 (2012) 1–10, https://doi.org/10.1155/2012/897127.

[33] M.A. Awadallah, B. Venkatesh, Bacterial foraging algorithm guided by particle swarm optimization for parameter identification of photovoltaic modules, Can. J. Electr. Comput. Eng. 39 (2016) 150–157, https://doi.org/10.1109/CJECE.2016.2519763.

[34] A. Gjukaj, G. Kabashi, G. Pula, N. Avdiu, B. Prebreza, Re-design of load shedding schemes of the Kosovo power system, World Acad. Sci. Eng. Technol. 50 (2011) 257–261.

[35] B. Hoseinzadeh, M.H. Amini, C.L. Bak, Centralized load shedding based on thermal limit of transmission lines against cascading events, in: IEEE Power Energy Soc. Gen. Meet., IEEE Computer Society, 2018, pp. 1–5. https://doi.org/10.1109/PESGM.2017.8274404.

[36] S. Sharma, N.S. Velgapudi, K. Pandey, Performance analysis of IEEE 9 Bus system using TCSC, in: 2017 Recent Dev. Control. Autom. Power Eng. RDCAPE 2017, Institute of Electrical and Electronics Engineers Inc., 2018, pp. 251–256. https://doi.org/10.1109/RDCAPE.2017.8358277.

[37] W. Rahmouni, L. Benasla, Transient stability analysis of the IEEE 39-bus power system using gear and block methods, in: 2017 5th Int. Conf. Electr. Eng. - Boumerdes, ICEE-B 2017, Institute of Electrical and Electronics Engineers Inc., 2017, pp. 1–6. https://doi.org/10.1109/ICEE-B.2017.8192187.